Detecting time variations in gravity associated with climate change

Eric W. Leuliette[1] and R. Steven Nerem[1]
Center for Space Research, University of Texas at Austin, Austin, Texas, USA

Gary L. Russell
NASA Goddard Institute for Space Sciences, New York, New York, USA

Received 1 May 2000; revised 16 March 2001; accepted 31 August 2001; published 13 June 2002.

[1] General circulation models offer a way to estimate the impact of mass redistributions on the Earth's time-varying gravity field. In this way, the prospects for detecting climate signals in the gravity field by dedicated satellite gravity missions, such as Gravity Recovery and Climate Experiment (GRACE), can be assessed. Using monthly averaged fluid mass diagnostics from a coupled atmosphere-ocean model developed at the Goddard Institute for Space Studies (GISS), we have estimated geoid variations from the fundamental model mass components. From these estimates the seasonal geoid signals from sea level, snow, soil moisture, water vapor, and atmospheric mass can be compared to the estimated errors for GRACE. All of these seasonal mass flows from the GISS model are well above the preliminary GRACE measurement errors. In addition, mass flows with significant secular trends attributable to the model's simulated increase of greenhouse gases would, in principle, be detectable by GRACE. However, the interannual variability of mass flows may require longer time series of gravity data, pattern analysis, or modeling improvements in order to detect trends. *INDEX TERMS:* 1214 Geodesy and Gravity: Geopotential theory and determination; 1243 Geodesy and Gravity: Space geodetic surveys; 4556 Oceanography: Physical: Sea level variations; 1899 Hydrology: General or miscellaneous

1. Introduction

[2] The Gravity Recovery and Climate Experiment (GRACE), an approved Earth System Science Pathfinder mission, is designed to return high-resolution measurements of both the static and time variable components of the Earth's gravity field for 5 years beginning in November 2001 [*Tapley and Reigber*, 1998]. The GRACE mission will consist of two satellites separated by ~220 km in a polar orbit ~500 km above the Earth. The range between the satellites will be determined with a dual-frequency microwave ranging system. The gravity field of the Earth will be computed at roughly monthly intervals using a combination of satellite-to-satellite tracking, GPS, and onboard accelerometer data. The accelerometers will measure nongravitational accelerations acting on the satellites, principally due to atmospheric drag. Removal of these effects is crucial to operating the mission in the low orbit necessary to resolve the gravity field at wavelengths of a few hundred kilometers.

[3] GRACE is expected to recover changes in seafloor pressure at length scales of a few hundred kilometers and longer and at timescales of a few weeks and longer with accuracies approaching 0.1 mbar (1 mm equivalent water thickness) [*Wahr et al.*, 1998]. GRACE will also likely detect changes of continental water storage in most drainage basins at monthly or longer time steps [*Rodell and Famiglietti*, 1999] to within a few millimeters. Signal aliasing, instrument errors, atmospheric modeling errors, and the magnitude of the variations will be the primary limitations on the relative accuracy of the GRACE-derived estimates.

[4] High-altitude satellites such as LAGEOS have demonstrated time-varying gravity field at long spatial wavelengths can be attributed to mass redistribution within the Earth's system, especially in the atmosphere, hydrosphere, and oceans [*Chen et al.*, 1999; *Cazenave et al.*, 1999; *Nerem et al.*, 2000]. Little has been observed of the time-varying gravity field at shorter wavelengths. Climatic atlases and general circulation models offer ways to estimate the size of time-varying gravity signals from particular mass flows.

[5] The main purpose of this paper is to investigate the magnitude of climate variations predicted by a coupled atmosphere-ocean model on the Earth's time-varying gravity signal. We will also address the prospects of detecting seasonal and secular climate change signals by the GRACE mission.

2. GISS Atmosphere-Ocean Model

[6] The NASA Goddard Institute for Space Studies (GISS) global atmosphere-ocean model (AOM) was designed to

[1]Now at Colorado Center for Astrodynamics Research, University of Colorado, Boulder, Colorado, USA.

0148-0227/02/2001JB000404$09.00

investigate climate changes on decade to century timescales [*Russell et al.*, 1995]. The model does not use flux adjustments nor restoring forces. The most significant aspects of the model that could be freely varying but are specified instead are the fixed horizontal fractions of vegetation types, land ice, and lakes and the use of climatological lake temperatures and lake ice distributions. The ice temperatures of lakes are predicted by the model.

[7] The AOM includes a nine-layer atmosphere, a 13-layer ocean, a six-layer soil model, and four-layer models for sea ice and land ice. The horizontal resolution is 4° in latitude by 5° in longitude for both the atmosphere and ocean. The resolution for heat, water vapor, and salt is finer than the grid resolution because those quantities have both means and directional prognostic gradients inside each grid cell. This information is used in the advection by the linear upstream scheme, and atmospheric condensation and ocean vertical mixing are performed on 2° × 2.5° horizontal resolution. Water mass released by one reservoir is received by another.

2.1. Ocean Model

[8] The ocean model does not use the rigid lid nor Boussinesq approximations. The ocean pressure gradient force recognizes the atmospheric and sea ice pressure above it. Water mass is conserved as opposed to volume. Salt is conserved globally. Natural boundary conditions allow river flow, precipitation, and evaporation to increase or decrease the ocean mass of a column. The model has weak signals for El Nino-Southern Oscillation (ENSO) and the North Atlantic Oscillation, which are significant sources of interannual sea level variability but have relatively small variations in total column atmosphere plus ocean mass.

[9] In the current simulations, the "k profile parameterization" of *Large et al.* [1994] is used for ocean vertical mixing. This improvement increased the Atlantic heat transport, which allowed a stable sea ice cover in the Northern Hemisphere and reduced the temperature drift in the North Atlantic.

[10] Each grid box in the ocean model may have a fractional horizontal sea ice cover with a single depth. Sea ice is advected, and it rejects all salt. Sea ice is stable with a realistic seasonal cycle that compares well with observations. Interannual variability of sea ice is realistic in the Northern Hemisphere but excessive in the Southern Hemisphere.

2.2. Atmosphere Model

[11] A comprehensive radiation scheme includes all significant gases, cloud particles, and aerosols. A diagnostic cloud formulation scheme is used instead of a prognostic formulation. Thus all atmospheric water is stored in the form of vapor. Precipitation is determined diagnostically and compares well with observations.

[12] The atmospheric dynamics use a globally conserved atmospheric mass, use a dry equation of state, and ignore humidity. This globally conserved atmospheric mass is accumulated as a monthly diagnostic and is used in this study. Although this mass responds to dynamic and thermodynamic forces, its seasonal and secular changes ignore global water vapor changes that occur in the real atmosphere.

2.3. Land Surface Processes

[13] Each continental grid cell has fixed horizontal fractions of ground, land ice, and lakes. Water is stored in separate reservoirs for ground, land ice, lake ice, and liquid lakes. The first three can include variable snow mass. Excessive snow is compacted into ice over land ice, lake ice, or sea ice but not over ground.

[14] The ground component includes a new hydrology scheme [*Abramopoulos et al.*, 1988]. Surface and underground runoff is fed into the lake arrays which are also affected by precipitation and evaporation. Lake mass above the sill depth is transported downhill by a river routing scheme [*Miller et al.*, 1994] with globally optimized timing.

[15] Land ice reservoirs can compress snow into ice or melt ice indefinitely. Although simple ice calving is implemented from Antarctica, land ice dynamics are not programmed. Land ice variations would dominate the secular changes in mass reservoirs but are not included in this study because their monthly diagnostics were accumulated as mass changes, not as mean values as was done for the other reservoirs.

2.4. Simulations

[16] Starting from an observed atmospheric state, zero ocean currents, and climatological ocean temperature [*Levitus and Boyer*, 1994] and salinity [*Levitus et al.*, 1994] fields, the atmosphere-ocean model was spun up for 40 simulated years with constant 1950 atmospheric composition. From this spin-up state, three simulations were integrated from 1950 to 2099: a control simulation (C089) that continues the spin-up simulation, an experiment that uses observed greenhouse gases until 1990 and compounded 0.5% CO_2 annual increases thereafter (C090), and an experiment with C090 greenhouse gases plus varying tropospheric sulfate aerosols (SA)(C091) that were provided by UK Met [*Mitchell et al.*, 1995]. The C091 experiment results in a cooler climate than does C090 because sulfate aerosols increase significantly until the year 2050 with a slight decrease thereafter. The seasonal regional temperature changes for the past 40 years show strong positive spatial correlation between C090 minus C089 and the observations in the Northern Hemisphere. C091 minus C089 shows weaker correlations with observations which is attributed to the difference in spatial patterns of sulfate aerosols between the model and the real world [*Russell et al.*, 2000]. At some locations the model's increased aerosols can reverse the sign of the increased greenhouse gas forcing.

3. Seasonal Variations in the Control Simulation

[17] The Earth's global gravity field is often expressed as an expansion of geoid height (the equipotential surface corresponding to mean sea level over the oceans), $G(\phi, \lambda)$, into a sum of spherical harmonics:

$$G = R\sum_{l=0}^{\infty}\sum_{m=0}^{l}\overline{P}_{lm}(\sin\phi)[C_{lm}\cos(m\lambda) + S_{lm}\sin(m\lambda)], \quad (1)$$

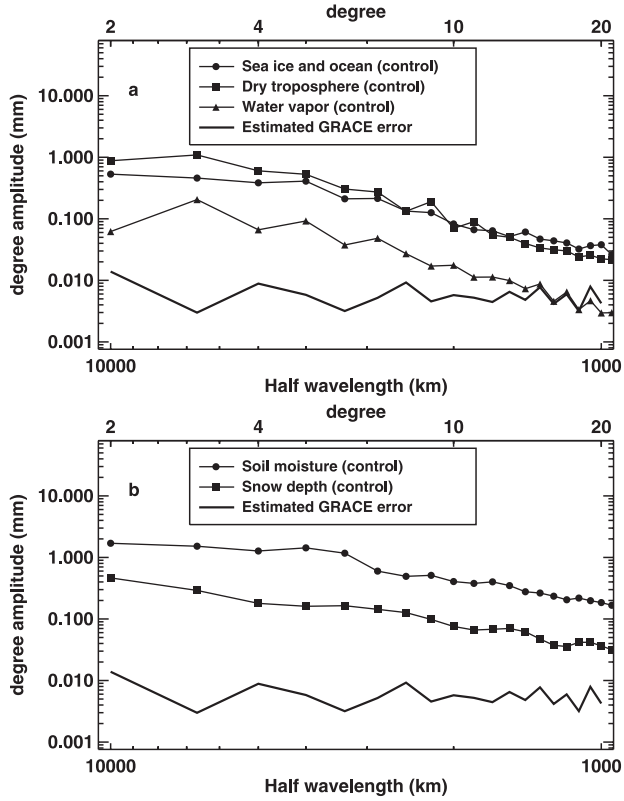

Figure 1. Degree amplitudes of the seasonaly varying geoid as deduced from the GISS AOM control simulation for (a) ocean and atmosphere and (b) surface mass changes.

where ϕ and λ are latitude and east longitude, R is the radius of the Earth, $\overline{P}_{lm}$ ($\sin\phi$) are the normalized associated Legendre functions, and C_{lm}, S_{lm} are the spherical harmonic coefficients of the gravity field. If the gravity field coefficients C_{lm} and S_{lm} are fit for cosine and sine components with an annual period (t = 0 on 1 January), then a space/time degree amplitude can be defined as

$$G_l = \frac{R}{\sqrt{2}}\sqrt{\sum_m \left(C_{lmc}^2 + S_{lmc}^2 + C_{lms}^2 + S_{lms}^2\right)}, \qquad (2)$$

where C_{lmc} and S_{lmc} are the cosine coefficients and C_{lms} and S_{lms} are the sine coefficients [*Wahr et al.*, 1998].

[18] Assuming that there are no net mass changes in the total Earth system (i.e., degree l = 0 terms = 0), the time-varying change in the geoid can be calculated as

$$\Delta G(\phi,\lambda) = \frac{3R\rho_w}{\rho_{\text{avg}}}\sum_{l=1}^{\infty}\sum_{m=0}^{l}\overline{P}_{lm}(\sin\phi)\frac{1+k_l}{2l+1}[\Delta C_{lm}\cos(m\lambda) + \Delta S_{lm}\sin(m\lambda)], \qquad (3)$$

where ρ_w is the density of water ($\approx$1000 kg/m^3), ρ_{avg} is the average density of the Earth (= 5517 kg/m^3), k_l is the load Love number of degree l, and ΔC_{lm} and ΔS_{lm} are time-varying spherical harmonic geoid coefficients [*Farrell*, 1972]. We have calculated the degree amplitude for the seasonally varying components of each mass field (ocean, globally conserved atmosphere, water vapor, snow, and soil moisture) of the control simulation using a least squares fit over model years 2001–2050. These results are plotted in Figure 1. Table 1 summarizes the amplitudes and phases of the low degree and order contributions of each mass field to the seasonally varying geoid.

[19] Preliminary estimates of the GRACE instrument errors for a single 30-day average [*Kim et al.*, 1999] can be extended to a one-year averaging period, assuming that the errors are uncorrelated between months. A covariance error analysis for simultaneously fitting cosine and sine terms with an annual period to the geoid coefficients shows that the uncertainty in each seasonally varying component is equal to the 30-day instrument error multiplied by $\sqrt{2/N}$, where N = 365/30 is the number of GRACE measurements per year of data. This uncertainty is shown in Figure 1. These estimates for GRACE instruments errors are derived from simulations and do not include any spatial averaging.

[20] The magnitudes of seasonally varying geoid changes from both the ocean, atmospheric mass, and soil moisture are somewhat larger than those reported by *Wahr et al.* [1998]. Surprisingly, the GISS AOM control simulation indicates that geoid changes attributable to variations in the ocean dominate atmospheric mass at wavelengths <2000 km (Figure 1a). Geoid changes due to soil moisture and snow (Figure 1b) originate from similar spatial geometries: continental regions with large seasonal variations in precipitation. Globally, geoid changes from soil moisture variations are an order of magnitude larger than those from snow, which is consistent with climatology.

[21] The spatial variations of the seasonally-varying geoid calculated using (3) for the GISS control simulation for soil moisture, snow, and ocean are shown in Figure 2. The magnitude and spatial scale of the geoid changes for soil moisture and to a lesser extent the oceans are similar to those found by *Wahr et al.* [1998]. The sine component of the soil moisture (Figure 2a) includes the largest seasonally varying features with +11 mm over central Asia and north central North America and −9 and −8 mm over western Africa and Southeast Asia, respectively. The seasonally varying geoid contributions from the ocean (Figure 2c) have amplitudes <3 mm. The sine contribution is dominated by a mass exchange from the Indian Ocean to the Mediterranean and Antarctica. The mass exchanges in the cosine contribution are more complicated, with transfers from the western and eastern equatorial Pacific and Middle East to

Table 1. Seasonal Geoid Variation in Control Simulation for 2001–2050[a]

	Ocean	Atmosphere	Water Vapor	Snow	Soil Moisture
C_{20}	(0.36, 42)	(0.44, 301)	(0.07, 217)	(0.67, 75)	(2.44, 73)
C_{21}	(0.32, 239)	(0.36, 247)	(0.01, 229)	(0.15, 83)	(0.58, 124)
S_{21}	(0.50, 343)	(1.13, 354)	(0.05, 363)	(0.22, 266)	(0.59, 251)
C_{22}	(0.42, 43)	(0.43, 196)	(0.02, 5)	(0.13, 265)	(0.24, 245)
S_{22}	(0.21, 216)	(0.33, 347)	(0.02, 14)	(0.03, 75)	(0.64, 12)
C_{30}	(0.61, 317)	(1.56, 147)	(0.32, 47)	(0.33, 71)	(1.31, 95)
C_{40}	(0.35, 131)	(0.59, 351)	(0.05, 30)	(0.02, 78)	(0.47, 248)

[a] The units of amplitude component are normalized geoid coefficients $\times 10^{-10}$. Units of phase component are day of maximum signal.

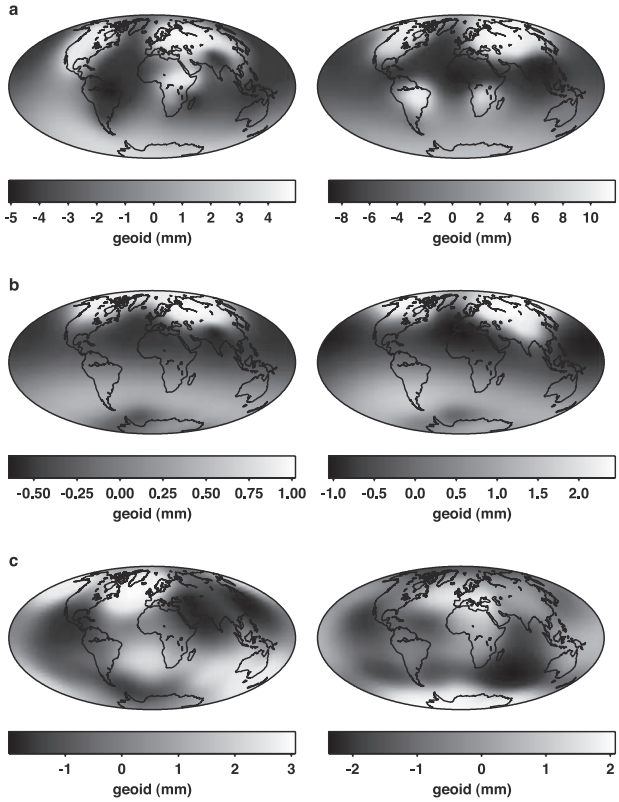

Figure 2. Contributions to the seasonally varying geoid component, as estimated from the GISS AOM control simulation for mass changes in (a) soil moisture, (b) snow, and (c) ocean. (left) Cosine component and (right) sine component are with $t = 0$ on 1 January. See color version of this figure at back of this issue.

the North Pacific, North Atlantic, and the Southern Ocean in the eastern hemisphere.

4. Impact of Climate Change

[22] Each model simulation can develop slight climate drifts caused by the continual accumulation of heat or salt at certain locations. Because these accumulations are consistent between simulations, subtracting the model control simulation from the two climate change simulations cancels most of the model climate drift, allowing the impact of climate change to be separated out. For simplicity, we designate the monthly difference between the simulation with increasing greenhouse gases (C090) and the control simulation (C089) as the greenhouse gas (GHG) experiment. Similarly, we designate the monthly difference between the simulation with increasing greenhouse gases and aerosols (C091) and the control simulation as the GHG + SA experiment. Because the Caspian Sea, an enclosed basin, produces anomalously large changes in mass, we have deleted it from the following analyses.

[23] We are interested in estimating the effects of global, long-term climate change on the time-varying geoid. For each mass field this requires the separation of a spatial pattern of decadal changes in the model's mass distribution from the shorter-period variability. Fitting linear trends to

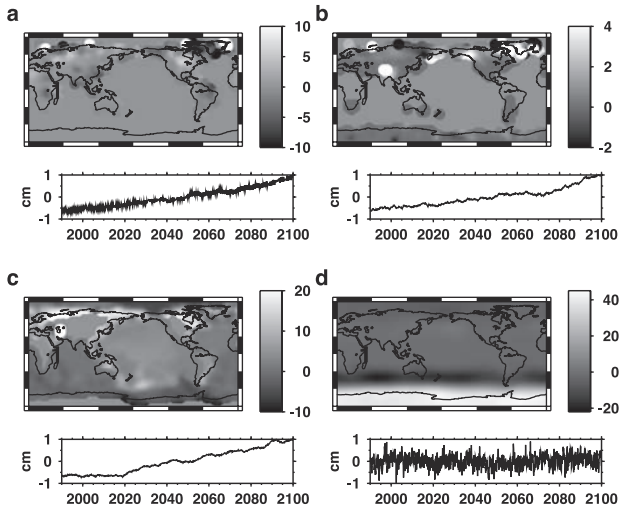

Figure 3. Spatial patterns and temporal coefficient of the first EOFs from the GHG + SA experiment for (a) soil moisture, (b) snow, (c) ocean mass, and (d) atmospheric mass changes. The units are the thickness of the equivalent water mass. Note that the change in ocean height depicts only sea level variation due to mass changes, not thermal expansion. See color version of this figure at back of this issue.

the raw mass field would determine local, transient changes in climate (as is the case when fitting trends to short periods of sea level data). Empirical orthogonal functions (EOFs) can be used to globally low-pass filter the mass fields, isolating a spatial pattern of climate change. The first EOF of each field in GHG and GHG + SA experiments for 1990–2099 isolates the spatial pattern of maximum variability (see Figure 3 for the GHG + SA mass fields). Table 2 lists the fraction of total variance explained by the first EOFs. In all GHG fields, except for atmospheric mass, the time series associated with the first EOF is largely a secular trend with interannual variations. (No time series of the atmospheric mass shows a significant trend.) The first EOF of GHG water vapor includes a trend in its time series and has twice the variance of the second mode EOF. The first EOF of GHG + SA water vapor includes no significant trend, and not surprisingly, the time series of the higher modes explain roughly the same fraction of the variance as the first. We have least squares fit the trend of the first EOF time series for each mass field over the period from 2001 to 2005, the anticipated duration of GRACE. The explained variance about the secular trends for each field in terms of total field variance are listed in Table 2.

Table 2. Fraction of Variance Explained by the First EOF[a]

	1990–2099		Trend in Mode 2001–2005	
Mass Field	GHG	GHG + SA	GHG	GHG + SA
Ocean	89.6	85.2	87.3	77.4
Snow	99.6	67.6	98.0	61.3
Soil moisture	98.5	66.4	97.0	59.2
Water vapor	10.6	5.5	7.8	0.2
Atmosphere	40.0	41.9	0.0	1.8

[a] Units are percent.

Table 3. Trends in Geoid Variation for 2001–2005 for the GHG + SA Experiment[a]

	Ocean	Snow	Soil Moisture
C_{20}	0.06 (0.09)	0.03 (0.05)	0.11 (0.17)
C_{21}	−0.08 (−0.13)	−0.02 (−0.04)	−0.07 (−0.12)
S_{21}	−0.12 (−0.18)	−0.05 (−0.09)	−0.17 (−0.27)
C_{22}	−0.04 (−0.06)	−0.05 (−0.07)	−0.15 (−0.24)
S_{22}	0.06 (0.10)	0.01 (0.01)	0.02 (0.04)
C_{30}	−0.05 (−0.07)	−0.01 (−0.01)	−0.02 (−0.03)
C_{40}	−0.03 (−0.05)	−0.01 (−0.02)	−0.04 (−0.06)

[a] The units of each component are in mm/yr, values in parentheses are normalized geoid coefficient $\times 10^{-10}$/yr.

[24] The major differences between each of the climate experiments is apparent in the resulting spatial distributions of the mass fields. For example, in the GHG experiment a secular change in water vapor is present, which enhances the effects of climate change. The spatial pattern of the first EOF shows the secular redistribution as an increase in mass over the Equatorial regions and a decrease in mass mostly over Antarctica (not shown). The results in the GHG + SA experiment illustrate the effect of aerosols (i.e., no significant secular trend in long-term water vapor mass redistributions).

[25] In the GHG experiment a distinct trend in ocean mass transfer is established by 2001 (not shown). The model shows mass loss at the polar ice cap and gain mostly in the Pacific. In the GHG + SA experiment, this trend begins around 2020 (Figure 3c).

[26] The secular component of the first EOFs (Figure 3) were used to calculate degree amplitude coefficients of the gravity field, analogous to the method used to calculate the amplitudes of the seasonal variations. Table 3 lists the contribution of each mass field to the trend in the low degree and order components of the geoid. Figure 4 shows the results of these calculations (in mm/yr). Note that the GRACE error estimates differ from those in the seasonal case. Here we have assumed that secular trends will be computed with 5 years of monthly gravity fields and that the errors are uncorrelated from month to month. The uncertainty in the trend (in change of height per year) computed by least squares can be estimated by multiplying the 30-day instrument error estimates by $\sqrt{n^3/12^3}$, where n is the number of months of data.

[27] Using the secular trend in the time-varying geoid components, (3) can be used to calculate the impact of climate change on the geoid. Figure 5 illustrates the trends in the

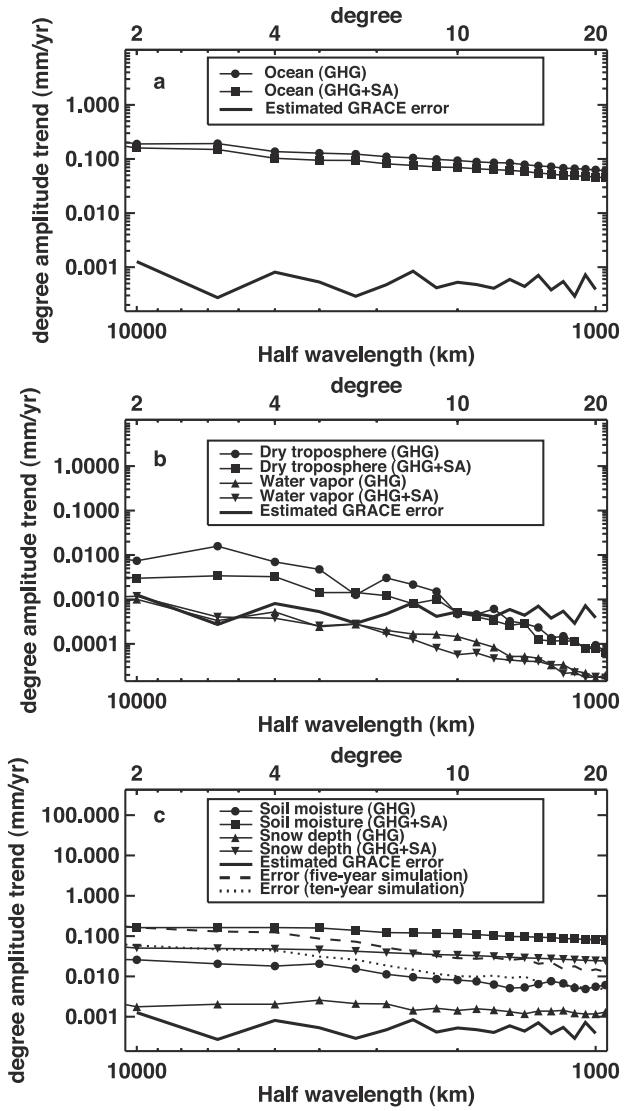

Figure 4. Trends in the geoid as deduced from the GISS AOM climate experiments for (a) ocean, (b) atmosphere, and (c) surface mass changes. Error estimates from instrument uncertainties, a GFDL hydrological model and postglacial rebound errors are plotted as dashed and dotted lines.

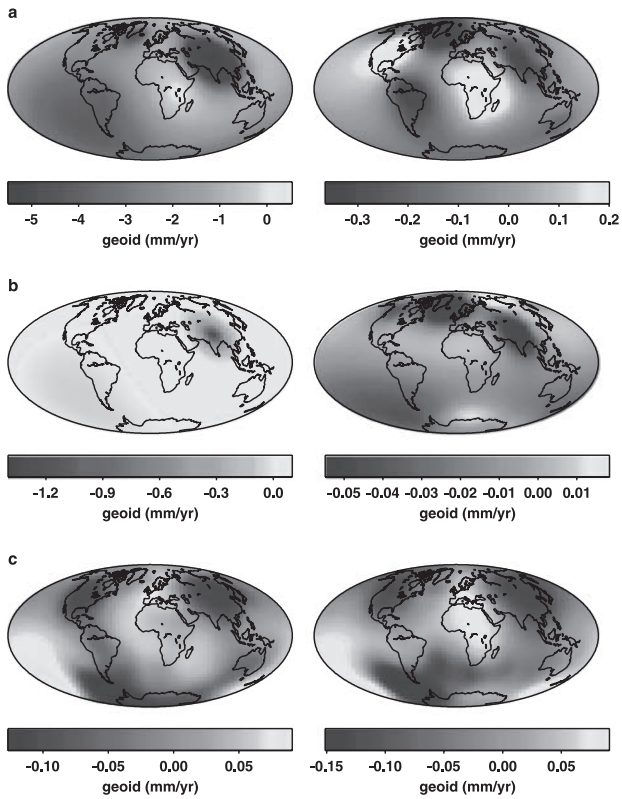

Figure 5. Contributions to the secular trend in the geoid as estimated from (left) the GISS AOM GHG experiment and (right) the GHG + SA experiment for mass changes in (a) soil moisture, (b) snow, and (c) ocean. See color version of this figure at back of this issue.

geoid from soil moisture, snow, and ocean mass for both the GHG and the GHG + SA experiments. The slower rates of climate change in the GHG + SA versus the GHG experiment can be seen in geoid impact from the trends in soil moisture and snow (Figures 5a and 5b). The trends resulting from the GHG + SA experiment are over an order of magnitude smaller than those from the GHG experiment. For soil moisture the spatial patterns from each experiment are distinct. The trend over North America is negative in the GHG experiment and is positive in the GHG + SA experiment. Changes in Himalayan snow mass dominate the secular geoid changes from the GHG experiment (Figure 5b). Otherwise, the spatial patterns between the GHG and GHG + SA experiment differ only in magnitude, not structure.

5. Recovery of Secular Trends

[28] At least four sources of uncertainty will contribute errors to recovering the trend in the geoid from climate variations. These include instrument uncertainty, postglacial rebound, interannual variability, and temporal aliasing.

[29] Postglacial rebound (PGR) is a secular change in the Earth's geoid which is the response of the solid Earth to the melting of ice at the end of the last ice age, and several models have been developed to describe the effect [*Han and Wahr*, 1995; *Lambeck*, 1990; *Tushingham and Peltier*, 1991]. In fact, one of the goals of the GRACE mission is to better constrain the viscosity profile of the mantle to improve PGR models. Depending on the lower mantle viscosity profile chosen, a 20–40% difference in geoid perturbation can result. To estimate the uncertainty in PGR modeling, we have taken the difference between crustal rebound rates predicted from PGR model simulations with lower mantle viscosities of 1×10^{22} Pa s and 5×10^{22} Pa s, respectively. Upper mantle viscosity is fixed at 1×10^{21} Pa s, and lithospheric thickness is 120 km in both models [*Han and Wahr*, 1995].

[30] The GISS AOM's strengths are its ability to simulate seasonal and secular changes in climate. However, interannual variations of continental water storage have large fluctuations at many spatial scales, similar to the problem of estimating secular sea level change using satellite altimetry [*Nerem et al.*, 1999]. Large, unmodeled interannual changes would increase the uncertainty in recovering the secular change in the geoid over the 5-year duration of the GRACE mission. To assess the impact of these interannual fluctuations on the recovery of secular trends in the geoid, we have used a terrestrial water storage data set generated from a Geophysical Fluid Dynamics Laboratory (GFDL) general circulation model [*Milly and Dunne*, 1994] to calculate the root-mean-square (RMS) amplitude of the interannual variations. We least squares fit and removed the seasonal variations from daily values of the GFDL model snow, soil moisture, and runoff fields. We used a boxcar filter to smooth variations <1 year. We then calculated the RMS change in the geoid from these mass fields over simulated 5- and 10-year periods.

[31] Because GRACE is expected to produce a complete geoid roughly once per month, higher-frequency mass variations in the ocean and atmosphere will be aliased into the time-varying geoid signal deduced from GRACE data. This is especially the case for diurnal mass variations, some of which can be well modeled. This aliasing, which will affect the recovery of seasonal and secular changes, is an active area of research.

[32] The combined error in secular trend recovery from instrument uncertainty, PGR error, and combined GFDL interannual variations is shown in Figure 4c. The effect of these errors is dependent both on the length of the available time series and the extent of the spatial averaging. We have simulated the uncertainties in the secular trend recovery for two cases: a single GRACE mission (5 years) and GRACE followed by a comparable mission (10 years). In both cases we have assumed a time sampling of 1 month and have not accounted for errors from temporal aliasing.

[33] The simulated uncertainties indicate that a 5-year GRACE mission could recover the secular trends in soil moisture mass variations at spatial scales of 1000–5000 km as predicted by the GHG + SA experiment (Figure 4c). The introduction of aerosols in the GHG + SA experiment results in continental-scale changes in precipitation that lead to significant secular trends in soil moisture content. At hemispheric scales the uncertainties of interannual variations are of the same order as the predicted trends, making unambiguous discrimination of the trends difficult. A 5-year mission could also be expected to recover the trends predicted by GHG + SA experiment's large changes in snow depth at wavelengths <1200 km. Ten years of GRACE-quality gravity data could recover the trend predicted by the GHG experiment for soil moisture mass changes at wavelengths >2000 km. Secular trends in snow depth predicted by the GHG experiment are 1–2 orders of magnitude 2 small to be unambiguously detected by even 10 years of GRACE-quality data.

6. Conclusions

[34] The seasonally varying gravity signals predicted by the GISS AOM for ocean, atmosphere, soil moisture, and snow mass changes are well above the preliminary GRACE measurement errors at half wavelengths ranging from 1000 to 10,000 km. GRACE measurements will likely provide a useful boundary condition for seasonal mass variations in coupled climate models.

[35] Mass flows with significant secular trends as calculated from differences in the model simulations have been used to estimate the secular change in the geoid due to climate change over 5 years. These mass redistributions should be detectable by GRACE in principle, although these Earth system components cannot be separated using GRACE data alone. However, variations in the spatial characteristics of each of the components may allow for their discrimination. Knowledge of the secular variations in gravity could be used for constraining future coupled atmosphere-ocean climate models. In addition, the effect of the aliasing of diurnal mass variations in the ocean and atmosphere from monthly sampling on the determination of interannual periods is a concern.

[36] One of the challenges in exploiting satellite gravity measurements for studying climate change will be the separation of signals, especially secular changes, from

variations such as postglacial rebound, since satellite measurements provide the total observed variation due to all the Earth system components. PGR can probably be modeled sufficiently to distinguish its gravity signal from mass shifts due to climate change. Interannual variability of mass flows may require longer time series of gravity data, pattern analysis, or ocean and atmosphere modeling improvements in order to detect trends. The results from the GISS AOM simulations indicate that GRACE may better able to unambiguously detect climate change signals at wavelengths shorter than the 1000 km limit of the model. Recent higher-resolution climate simulations (e.g., the Department of Energy's Parallel Climate Model) may help to clarify this in the future. (Graphs and data of the atmosphere-ocean model simulations used in this paper are available at http://aom.giss.nasa.gov.)

[37] **Acknowledgments.** We are grateful to J. M. Wahr for providing software to compute Stoke's coefficients and postglacial rebound estimates, C. Milly and K. Dunne for providing the GFDL terrestrial water data set, and S. Bettadpur for providing the GRACE error estimates. We also thank C. Wilson for helpful discussions and A. Cazenave, J. O. Dickey, and J. M. Wahr for useful comments and suggestions in their reviews. This work was supported by a NASA Solid Earth and Natural Hazards science investigation and a NASA EOS Interdisciplinary Science Investigation, NAG5-6309, Earth Systems Dynamics.

References

Abramopoulos, F., C. Rosenzweig, and B. Choudhury, Improved ground hydrology calculations for global climate models (GCMs): Soil water movement and evapotranspiration, *J. Clim.*, *1*, 921–941, 1988.

Cazenave, A., F. Mercier, F. Bouille, and J. M. Lemoine, Global-scale interactions between solid Earth and its fluid envelopes at the seasonal time scale, *Earth Planet. Sci. Lett.*, *171*, 549–559, 1999.

Chen, J. L., C. R. Wilson, R. J. Eanes, and B. D. Tapley, Geophysical contributions to satellite nodal residual variation, *J. Geophys. Res.*, *104*, 23,237–23,244, 1999.

Farrell, W. E., Deformation of the Earth by surface loading, *Rev. Geophys.*, *10*, 761–797, 1972.

Han, D., and J. Wahr, The viscoelastic relaxation of a realistically stratified Earth and a further analysis of post-glacial rebound, *Geophys. J. Int.*, *120*, 287–311, 1995.

Kim, J. R., P. J. Roesset, S. V. Bettadpur, and B. D. Tapley, Simulations of the Gravity Recovery and Climate Experiment (GRACE) mission, *Spaceflight Mech.*, *102*, 99–144, 1999.

Lambeck, K., Glacial rebound, sea level change, and mantle viscosity, *Q. J. R. Astron. Soc.*, *31*, 1–30, 1990.

Large, W. G., J. C. McWilliams, and S. C. Doney, Oceanic vertical mixing: Review and a model with non-local boundary layer parameterization, *Rev. Geophys.*, *32*, 363–403, 1994.

Levitus, S., and T. P. Boyer, *World Ocean Atlas 1994*, vol. 4, *Temperature, NOAA Atlas NESDIS 4*, Natl. Oceanic and Atmos. Admin., Silver Spring, Md., 1994.

Levitus, S., R. Burgett, and T. P. Boyer, *World Ocean Atlas 1994*, vol. 3, *Salinity, NOAA Atlas NESDIS 3*, Natl. Oceanic and Atmos. Admin., Silver Spring, Md., 1994.

Miller, J. R., G. L. Russell, and G. Caliri, Continental scale river flow in climate models, *J. Clim.*, *7*, 914–928, 1994.

Milly, P. C. D., and K. A. Dunne, Sensitivity of the global water cycle to the water-holding capacity of land, *J. Clim.*, *7*, 506–526, 1994.

Mitchell, J. F. B., R. A. Davis, W. J. Ingram, and C. A. Senior, On surface temperatures, greenhouse gases and aerosols: models and observations, *J. Clim.*, *8*, 2364–2386, 1995.

Nerem, R. S., D. P. Chambers, E. W. Leuliette, G. T. Mitchum, and B. S. Giese, Variations in global mean sea level associated with the 1997–1998 ENSO event: Implications for measurements long term sea level change, *Geophys. Res. Lett.*, *26*, 3005–3008, 1999.

Nerem, R. S., R. J. Eanes, P. Thompson, and J. L. Chen, Observations of annual variations of the Earth's gravitational field using satellite laser ranging and geophysical models, *Geophys. Res. Lett.*, *27*, 1783–1786, 2000.

Rodell, M., and J. S. Famiglietti, Detectability of variations in continental water storage from satellite observations of the time dependent gravity field, *Water Resour. Res.*, *35*, 2705–2723, 1999.

Russell, G. L., J. R. Miller, and D. Rind, A coupled atmosphere-ocean model for transient climate change, *Atmos. Ocean*, *33*, 683–730, 1995.

Russell, G. L., J. R. Miller, D. Rind, R. A. Ruedy, G. A. Schmidt, and S. Sheth, Comparison of model and observed regional temperature changes during the past 40 years, *J. Geophys. Res.*, *105*, 14,891–14,898, 2000.

Tapley, B. D., and C. Reigber, GRACE: A satellite-to-satellite tracking geopotential mapping mission, *Eos Trans. AGU*, *80*(49), Fall Meet. Suppl. F208, 1998.

Tushingham, A. M., and W. R. Peltier, ICE-3G: A new global model of late Pleistocene deglaciation based upon geophysical predictions of postglacial relative sea level change, *J. Geophys. Res.*, *96*, 4497–4523, 1991.

Wahr, J., M. Molenaar, and F. Bryan, Time-variability of the Earth's gravity field: Hydrological and oceanic effects and their possible detection using GRACE, *J. Geophys. Res.*, *103*, 30,229–32,205, 1998.

E. W. Leuliette and R. S. Nerem, Colorado Center for Astrodynamics Research, University of Colorado at Boulder, 431 UCB, Boulder, CO 80309-0431, USA. (eric.leuliette@colorado.edu; nerem@colorado.edu)

G. L. Russell, NASA Goddard Institute for Space Sciences, 2880 Broadway, New York, NY 10025, USA. (russell@giss.nasa.gov)

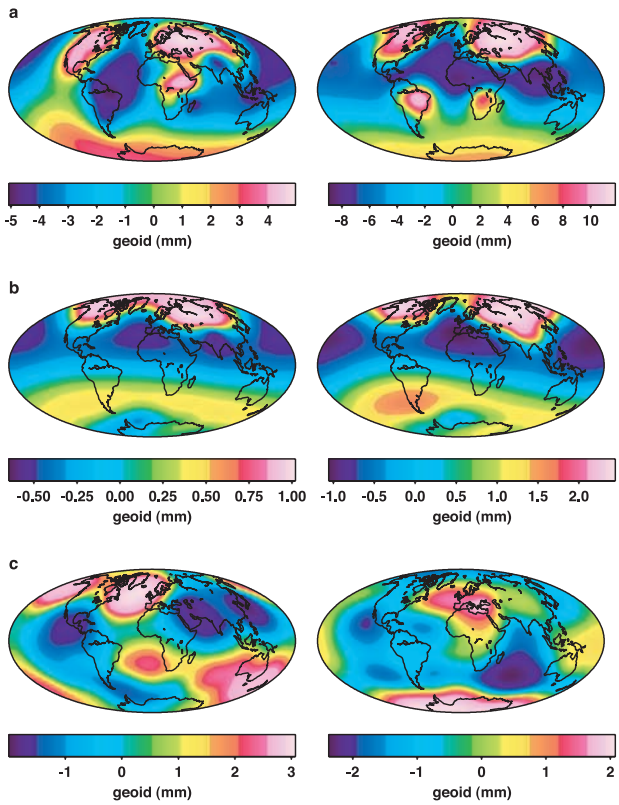

Figure 2. Contributions to the seasonally varying geoid component, as estimated from the GISS AOM control simulation for mass changes in (a) soil moisture, (b) snow, and (c) ocean. (left) Cosine component and (right) sine component are with $t = 0$ on 1 January.

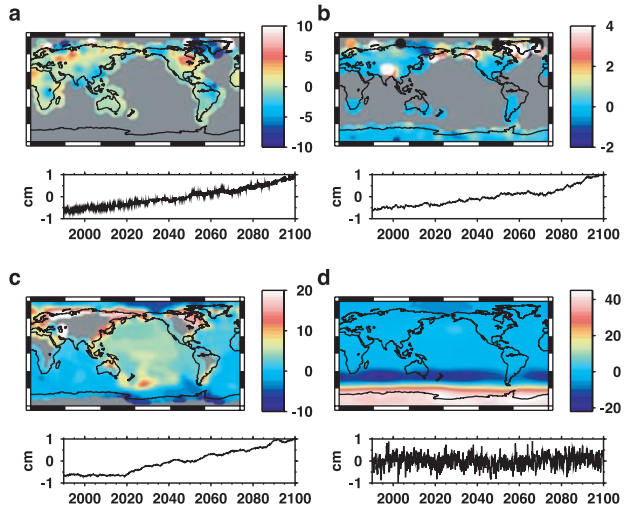

Figure 3. Spatial patterns and temporal coefficient of the first EOFs from the GHG + SA experiment for (a) soil moisture, (b) snow, (c) ocean mass, and (d) atmospheric mass changes. The units are the thickness of the equivalent water mass. Note that the change in ocean height depicts only sea level variation due to mass changes, not thermal expansion.

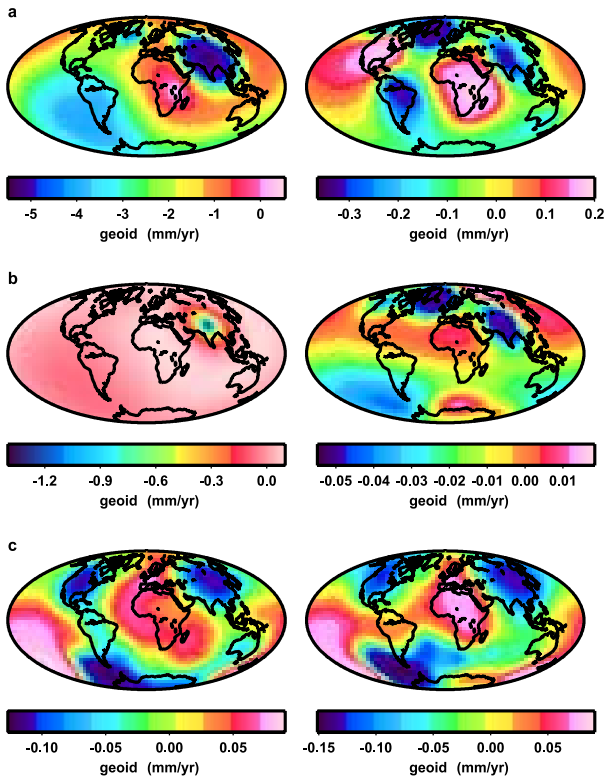

Figure 5. Contributions to the secular trend in the geoid as estimated from (left) the GISS AOM GHG experiment and (right) the GHG + SA experiment for mass changes in (a) soil moisture, (b) snow, and (c) ocean.